This is the preprint version of the paper:

D. Sterpi, G. Tomaselli, A. Angelotti, Energy performance of ground heat exchangers embedded in diaphragm walls: Field observations and optimization by numerical modeling, Renewable Energy 2020, 147 (2), 2748-2760 https://doi.org/10.1016/j.renene.2018.11.102

Link for the published paper:

https://authors.elsevier.com/a/1a9ww3QJ-dXXpe

Energy performance of ground heat exchangers embedded in diaphragm walls: field observations and optimization by numerical modelling

D. Sterpi[a], G. Tomaselli[b], A. Angelotti[b]*

[a] Department of Civil and Environmental Engineering, Politecnico di Milano, Italy

[b] Energy Department, Politecnico di Milano, Italy

*corresponding author: adriana.angelotti@polimi.it

Abstract

Ground immersed structures thermally activated by embedded heat exchangers represent a solution for building climatization, that combines efficiency, sustainability and cost saving. However, the performance of thermally activated diaphragm walls is influenced by key factors that still require insights, such as the layout of the exchanger pipe, the ratio between exposed and fully immersed parts of the wall, and the variable thermal condition at the excavation side. In this paper, these aspects are investigated first with reference to a full scale monitored diaphragm wall. From the field observations a finite element model is set up, validated by sensitivity analyses and calibrated on the monitoring data. The model is then used to attempt an optimization of the exchanger pipe layout. For given structure, ground conditions, thermal inputs and properties, the energy performance can be improved by limiting the thermal interference between pipe branches circulating fluid at different temperatures, and by taking advantage of the fully immersed part of the wall, on both faces in direct contact with the soil. A suggestion is given for enhanced pipe layouts that meet these requirements and lead to up to a 15.8% increase of exchanged heat rate for the studied case.

Keywords: Ground source heat pump; Thermo-active diaphragm wall; Energy geostructure; Ground heat exchanger; Monitoring; Finite Element model.

1. Introduction

Ground Source Heat Pumps (GSHP) are energy efficient and environmental friendly climatization systems for buildings. They experienced a remarkable growth in the years 2010-15, when the installed capacity worldwide grew 1.52 times and the annual energy use increased 1.63 times [1]. Among direct uses of geothermal energy, they are the most widespread, accounting for 70.90% of the installed capacity and 55.15% of the annual energy use in 2015. Moreover, the introduction of the Nearly Zero Energy Buildings concept by the EU EPBD Directive [2], constraining all new buildings to comply to the NZEB standard by 2020, is expected to further foster GSHP in Europe as one of the systems that can contribute to the target.

Despite the well-known advantages, GSHP suffer from the economic barrier of the relatively high initial capital cost, which is significantly affected by the excavation cost of the Ground Heat Exchanger (GHE). According to Blum et al. [3], who analyzed data regarding more than 1100 GSHP installed in Germany, for heating demands below 30 kW, the average cost for drilling and installing Borehole Heat Exchangers (BHE) is 11997 €, accounting for 51% of the average total cost, namely 23460 €.

The drilling cost can be substantially avoided if the GHE is embedded in the building foundations, already required for structural reasons. So-called thermo-active foundations or energy geostructures are piles, slabs, retaining walls or tunnel linings that work at the same time as structural elements and components of the GSHP system [4-6]. Among thermo-active foundations, energy piles are the most similar to conventional BHE. However, some

geometrical differences can be found, regarding the diameter (10-15 cm for BHE, up to 3 m for piles) and the depth (typically 100 m for BHE, rarely more than 40 m for piles), and leading to smaller depth-to-diameter ratios for piles compared to BHE. Although current design analysis tends to assume that the thermal response of piles is equivalent to that of BHE, specific issues regarding piles should be considered, such as the importance of axial effects on the long-term, the thermal interaction with the building, the large heat capacity of the pile [7]. Therefore, thermal and thermo-mechanical analysis of energy geostructures is an area of current activity and collaboration [7,8]. Analysis and design of energy foundation slabs and retaining walls is further complicated by the absence of cylindrical symmetry (which indeed does not hold even for piles in the presence of a groundwater flow) and by the role of the boundary condition acting on the excavation side of the energy structures. As far as diaphragm walls analysis for buildings is concerned, Sun et al. [9] propose a 2D heat transfer model that distinguishes between over and under the excavation line. Under the excavation line the wall faces the soil on both sides, while over the line the wall connects to soil on one side and to air on the excavation side. It has to be remarked however that, in real buildings applications, identifying the air temperature acting on the excavation side is not straightforward. As far as energy walls in tunnels are concerned, the importance of the tunnel/air void characteristics in the thermal response of thermo-active walls in cut-and-cover tunnels is also pointed out in [10] and a review of adopted average temperatures and heat transfer coefficients is discussed in [11]: thermal characterization of the boundary between the wall and the air void requires greater scrutiny, in order to ensure realistic predictions of energy performance.

Diaphragm walls offer in principle more possibilities compared to piles from the piping layout point of view. Xia et al. [12] compare experimentally the energy performance of 3 energy walls with W-shaped, improved W-shaped and single U-shaped piping, for different

inlet fluid temperatures and flow rates. They find that the W-shaped piping can exchange 25-40% more than single U-shaped, and that the improved W-shaped, where the distance between branch tubes on the soil side is enlarged, increases the heat transfer rate by 11% compared to W-shaped one. The U- and W- shaped layouts recall the classical piping layouts adopted in boreholes, while an original slinky pipe arrangement is adopted in the diaphragm walls of the Bulgari Hotel Knightsbridge London project [13]. Alternative piping layouts are studied by the Authors in a previous study [14] through a finite elements numerical model, although the modelling refers to an ideal diaphragm wall. A parametric thermal analysis is discussed by Di Donna et al [11], who highlight how the energy performance benefits from increasing the number of pipes and using concrete of enhanced thermal properties and, at the same time, how the possible temperature excess between the wall and the excavation is advantageous for heat extraction but detrimental for waste heat disposal.

Energy performance figures regarding thermo-active diaphragm walls based on field experience are generally lacking. Brandl [15] reports 30 W/m^2 for a pre-design evaluation of energy walls fully embedded in the soil, while Xia et al. [12] measure 33.6-68.4 W/m depending on the inlet fluid temperature and on the piping shape. Kurten et al. [16] report specific heat rates in the range 20-100 W/m for thermo-active seal panels tested in laboratory under different groundwater velocities. Heat rates are normalized either by the earth-contact area of the wall [15] or by the wall depth [12] or even by the pipe length [16].

Therefore, further efforts are necessary to assess experimentally the energy performance of thermo-active diaphragm walls, to model and analyze the influence of the boundary condition on the excavation side and to optimize the heat exchanger layout. In this paper all these aspects are investigated, starting from field observations on a monitored case study in Northern Italy. Experimental results are used to derive energy performance figures, to get fundamental insights into the behavior of the over and below excavation portions of the

diaphragm walls and to calibrate a finite element numerical model of the wall panel. By means of the developed numerical model the sensitivity of the heat transfer performance to key parameters is assessed and optimal piping layouts are identified, based on minimizing the thermal interference among branches and fully exploiting the soil embedded part of the wall.

2. System description

The case study refers to a 6-storey residential building located in Tradate, Varese, Italy (Figure 1). The building, completed in 2015, was designed as a low energy building with an energy efficient envelope, a high performance Heating Ventilation and Air Conditioning (HVAC) system and a building automation system. The HVAC system generation unit consists in a water-to-water polyvalent Ground Source Heat Pump (GSHP), providing heating, cooling and Domestic Hot Water (DHW) to the residential units, by using the ground and the groundwater as heat sources or sinks, depending on the season. Groundwater coupling is achieved by means of an extraction and an injection well, while ground coupling is obtained by means of thermo-active geostructures.

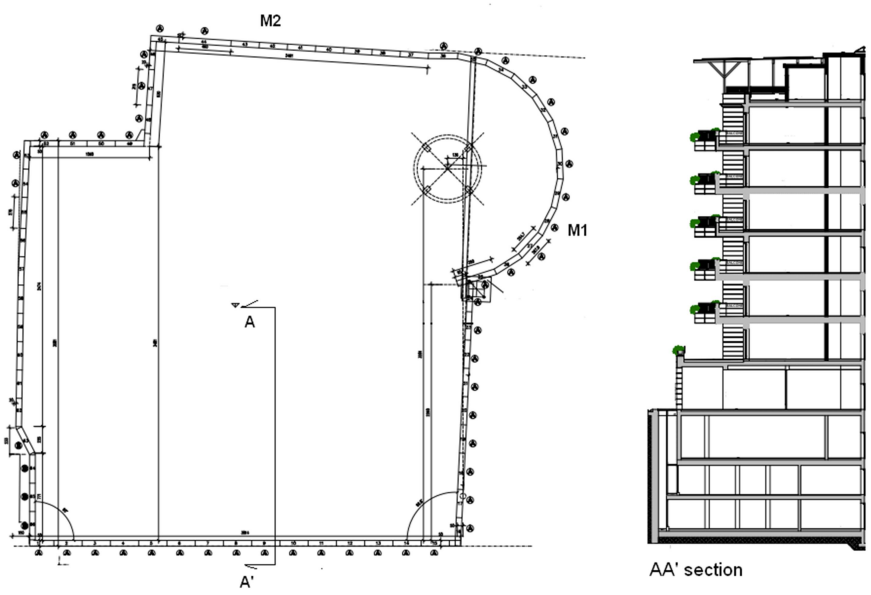

Figure 1. Left: Building underground storey layout showing the diaphragm wall panels along the perimeter, right: side view of the building along AA' section

To this regard the building perimeter is equipped with 66 diaphragm walls panels for an overall area of 2376 m^2 (Figure 1). Each panel, 2.4 m large and 0.5 m thick, is 15 m deep below the ground surface level and anchored to the ground by means of two 10 m long anchors. As it is shown in Figure 2, reporting the geometry of the typical diaphragm wall panel, the building base slab lies about 10 m below the surface, so that 1/3 the diaphragm wall area is fully immersed in the ground, the rest facing the ground on the external side and the building on the internal side (Figure 2). As it can be noticed from Figure 1, depending on the position on the building perimeter, diaphragm walls internal sides can either face directly the 3 underground storeys of the building dedicated to parking, or the parking ventilation air gap, or even the ramp to access the parking. Every diaphragm wall panel was equipped with 2 heat exchangers, namely 2 hydraulic loops, each 90 m long, made up with a HDPE pipe. The pipes were fastened from the inside to the reinforcement steel cages (2.4% steel bars area over the wall cross section) on the soil side and therefore have about 5-8 cm distance from the soil face (Figure 3). The resulting pipe layout consists in 6 vertical branches, about 15 m long and 16 cm distant from each other (sequentially named from A to F in the layout schematic view of Figure 7). Considering that the anchors heads as well as the concrete casting tubes are placed in the central portion of each diaphragm wall panel in order to minimize the risk to damage the heat exchangers, the latters were placed aside the central portion. Each diaphragm wall panel can thus be divided into 3 parts 0.8 m large, 2 thermo-active parts on the sides and a central part performing only the structural function (Figure 2). Besides the heat exchangers embedded in the diaphragm walls, the building base slab area (1689 m^2) is also equipped with heat exchangers on the soil side.

The ground survey on site revealed that the ground up to the excavation depth is mainly composed of gravelly sand with silt, with average porosity of 0.47. The upper 9.5 m are rather homogeneous, with a gravel content of 10-20%, a sand content of 60-70% and a silt content

of 15-20%. A coarser layer at 3-4.5 m is found, with an increase of gravel content to 20-30%. Below 9.5 m, the gravel content reaches about 35-40% and the sand content decreases to 45-50%, the silt content remaining rather uniform. A stable groundwater level was detected at about 9.7 m from the surface, although a saturated condition was identified in the coarser layer at 3-4.5 m below the surface. In the following analyses the basic hypothesis will be made that the soil is fully saturated and in drained conditions, given its coarse nature. The hydraulic gradient was qualitatively detected as very limited during the site survey.

The building and the HVAC system are monitored through a purposely devised data acquisition system by Tecnoel srl aiming to control the system operation and optimize the performance. In the framework of a collaboration between the construction firm F.lli Bertani and the Authors, the data acquisition system was expanded with a set of RTD temperature probes dedicated to the monitoring of two diaphragm wall panels, indicated as M1 and M2 in Figure 1. The temperature probes position in every monitored diaphragm wall is shown in Figure 2: they consist in 5 probes in the ground along the 1st anchor (named AS) and 11 probes embedded in the wall at different depths (5 on the soil side, named SS, and 6 on the excavation side, named ES). For the purpose of this study, the probes measuring the fluid temperature at the inlet and outlet of the diaphragm walls and of the slab collectors and the corresponding circulating flow rates were also considered. The measurement accuracy is estimated as 0.3°C and 10% for the temperatures and the flow rates respectively. Data are acquired every minute. From these measurements, the overall heat rate exchanged by each of the two thermo-active geostructures (diaphragm walls, slab) is derived as:

$$\dot{Q} = \dot{m}c\left(T_{f,out} - T_{f,in}\right) \quad (1)$$

where $\dot{m}$ is the measured mass flow rate, c the specific heat capacity of water, $T_{f,out}$ and $T_{f,in}$ the fluid outlet and inlet temperature. By integrating the heat rate over time the heat extracted from the ground on a monthly basis is obtained.

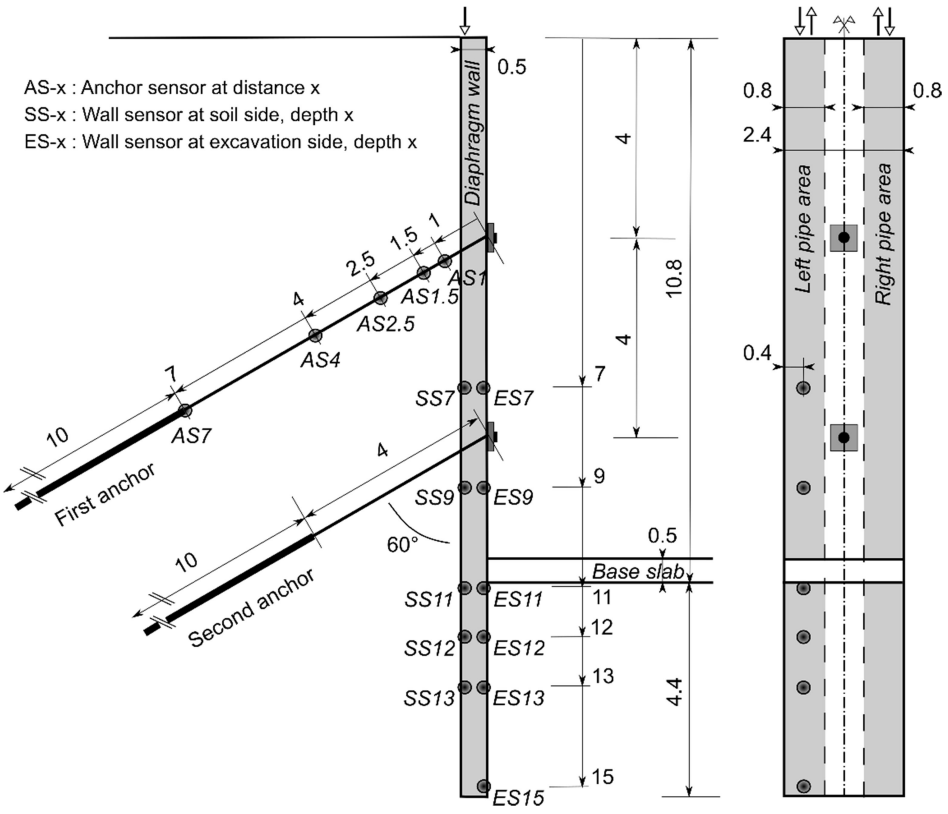

Figure 2. Diaphragm wall: side view (left) and frontal view from the excavation side (right); temperature probes positions and labels are shown.

Figure 3. The reinforcing cage and the heat exchanger pipe fastened to it.

3. Field observations results

Monitoring started in July 2015, although the HVAC system started to operate in a continuous and significant way only during winter 2015/16, providing space heating and DHW to the building. Therefore the analysis reported here is focused on a 4 months period, from December 2015 to March 2016. The heat extracted from the ground by the geostructures on a monthly basis is firstly used to derive monthly average heat rates. Then the average heat rates are properly normalized in order to derive performance figures comparable with literature. By normalizing for the overall area of the diaphragm walls (S_{dw} = 2376 m^2) or the base slab (S_{bs}= 1689 m^2), a comparison can be performed with Brandl [15], reporting 30 W/m^2 for diaphragm walls fully embedded in the soil and 10-30 W/m^2 for base slabs. In turn, by normalizing for the diaphragm wall depth, a comparison can be carried out with Xia et al. [12], who report a performance in the range 33.6-43.2 W/m, depending on the heat exchanger layout into the diaphragm wall, for 32°C fluid inlet temperature. The heat rates per unit surface of the geostructures are shown in Figure 4 and reported in Table 1, the latter showing also the heat rates per unit depth of the geostructures. Seasonal average heat rates per unit surface are 13.9 W/m^2 and 5.2 W/m^2 for the diaphragm walls and the base slab respectively, therefore the diaphragm walls heat exchange rate is on average 2.7 times larger than the one of the base slab. Such figures appear much lower than the references in [15], suggesting that ground heat exchangers installed in those geostructures that are only partially embedded in the soil may behave sensibly worse. Actually the diaphragm walls seasonal average heat rate per unit depth is 33.4 W/m, in good agreement with [12], where diaphragm walls are subject to a boundary condition more similar to the present case study, since the inside face of the walls is exposed to the building for the first 18.5 m out of 38 m of the walls depth. Therefore, although the diaphragm walls in the present case cannot be considered fully embedded in the soil, a simple and qualitative check of the consistency of our results with the literature value by Brandl [15]

can be carried out as follows. The diaphragm walls area can be modeled as the sum of the area below excavation level $S_{be} = \frac{1}{3} S_{dw}$ and the area over excavation level $S_{oe} = \frac{2}{3} S_{dw}$, the first one performing in un unknown way and the second one performing, in a first approximation, like the base slab i.e. exchanging 5.2 W/m^2. The latter is clearly a rough assumption, since the air flow on the inside face of the wall and on the upper surface of the base slab may be different, as well as the ground temperature field acting on the soil side of the two structures. However, if the overall resulting performance of 13.9 W/m^2 is considered as the average of the performance of the two parts, weighed by their pertinence areas, the performance of the portion below excavation results in 31.5 W/m^2, namely very close to 30 W/m^2.

	diaphragm walls		base slab
	q/S_{dw} (W/m^2)	q/H (W/m)	q/S_{bs} (W/m^2)
Dec	14.9	35.8	8.6
Jan	12.8	30.8	3.2
Feb	14.9	35.7	4.8
Mar	12.5	30.0	3.6
season	13.9	33.4	5.2

Table 1. Monitoring results: monthly and seasonal average heat rates per unit surface and unit depth of the geostructure

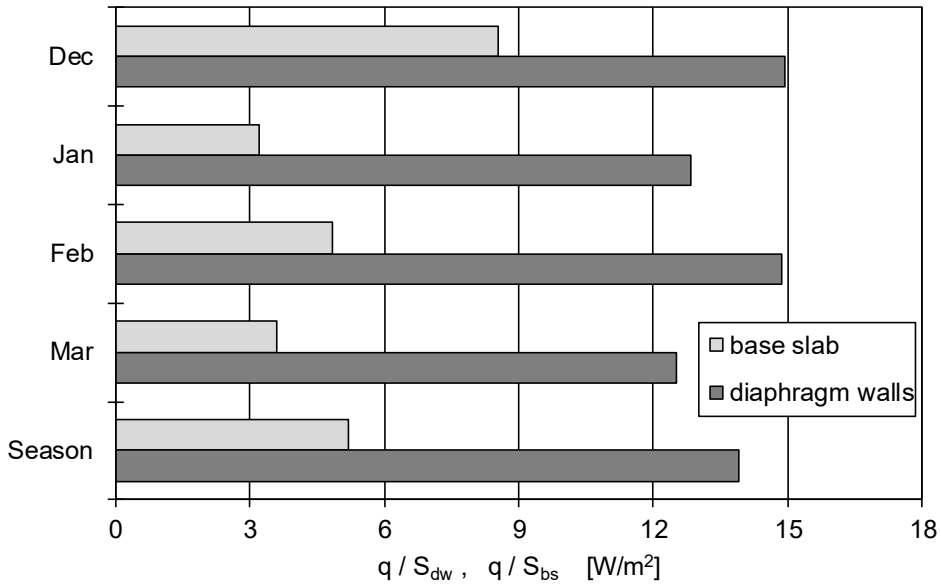

Figure 4. Monitoring results: monthly and seasonal average heat rates per unit surface of the diaphragm walls and of the base slab

Temperature profiles measured by the probes embedded in the two monitored diaphragm wall panels support the statement that the over excavation and the below excavation level portions of the energy geostructures behave differently. Figure 5 reports the temperatures measured during winter 2015/16 on the soil side (SS) and on the excavation side (ES) of one of the panels at depths of 7 m and 12 m, namely over and below excavation level. The temperature measured in the ground by the sensor AS7 on the 1st anchor (see Figure 2), being at about 7 m from the ground surface, is also shown for comparison. The SS probes lie in the same plane of the ground heat exchanger and therefore are highly influenced by the heat transfer fluid temperature. Below the excavation level the soil side temperature is generally lower than the excavation side temperature, both being lower than the undisturbed soil temperature that is estimated to about 13°C. Therefore both sides of the diaphragm wall panel are effective in harvesting heat from the ground. In turn, above the excavation level the soil side remains warmer than the excavation side at least until February 2016, suggesting that the heat

exchanger portion over the excavation is not able to intercept all the heat flowing from the surrounding ground to the building underground storeys.

In summary, field observations suggest that the overall diaphragm wall energy performance results from the combination of the below excavation and the above excavation portion performance, the latter being influenced by a critical boundary condition. In the present configuration of the heat exchangers embedded in the diaphragm walls, given the piping layout, the fluid path runs many times consecutively above and below the excavation level, possibly overriding the better performance of the lower portion with the worse one of the upper portion. Moreover, with respect to literature examples [10,12] the present piping layout appears very dense, with the inlet and outlet segments running near and with a mall distance between adjacent segments. A numerical model of the diaphragm wall panel is then created to identify the key parameters influencing the energy performance and to study alternative optimal piping configurations, able to minimize thermal interference within the pipe segments and to fully exploit the wall portion below excavation level.

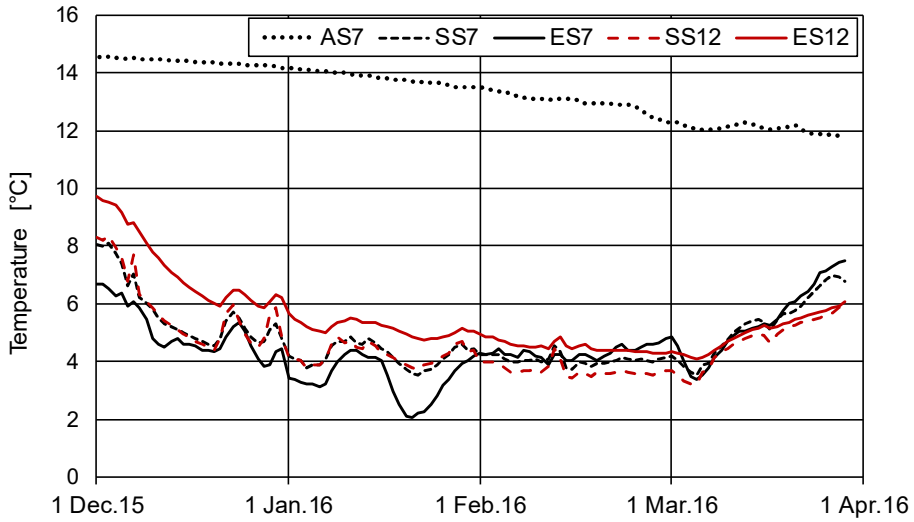

Figure 5. Monitoring results: temperature profiles from December 2015 to March 2016 at 7 m (over excavation level) and 12 m (below excavation level), within the ground (AS), on the soil side of the diaphragm wall panel (SS) and on the excavation side (ES).

4. Numerical modeling

4.1 Geometry and materials

Numerical analyses of the thermal behavior were performed using the finite element commercial code Abaqus v.6.14 [17], that allows to combine heat transfer mechanisms by conduction and by convection on distinct parts of the domain.

The modelling of the three-dimensional geometry of the case study takes advantage of the symmetries of the excavation area (Figure 1) and of the transversal symmetry plane of the wall panel (Figure 2), so that the entire domain consists of a three-dimensional slice, 1.2 m wide, corresponding to half of a single panel (Figure 6).

On the front and back faces, being symmetry planes, an adiabatic condition is prescribed. The same condition applies to the right lateral boundary, which is the central symmetry plane of the excavation, and to the left lateral boundary, which is considered sufficiently distant from the thermo-active wall and therefore unaffected by horizontal temperature gradients. At the ground surface and at the excavation boundaries (wall and slab) yearly cyclic variations of temperature are prescribed, based on atmospheric conditions monitored by the Regional Agency for Environmental Protection (ARPA-Lombardia), as it is described in Section 4.2. A constant and uniform temperature is assigned to the bottom face to represent a far-field undisturbed condition. The value of 13.4°C, equal to the mean value of the yearly cyclic temperatures at the ground surface, is chosen to maintain a global energy equilibrium.

Three parts of the domain are explicitly modelled, i.e. the reinforced concrete structures (diaphragm wall and base slab, as homogeneous bodies), the saturated soil and the volume occupied by the fluid filling the pipe. For simplifying the meshing process and limiting the number of elements: (i) the presence of the HDPE tube is neglected, (ii) the internal circular

section of the pipe (1.6 cm of diameter) is replaced by an equivalent square section (1.42 cm of side) and (iii) in the layout simpler square corners replace actual rounded folds (Figure 7). The resulting mesh consists of 45.610 nodes, with 237.511 4-node linear tetrahedron elements suited to heat conduction, for structures and soil, and 1.813 8-node hexahedron elements suited to forced convection, for the flowing fluid. The cross section of the pipe is modelled with one finite element, entailing that the fluid velocity, directed as the pipe axis, and the fluid temperature are uniform over the pipe section.

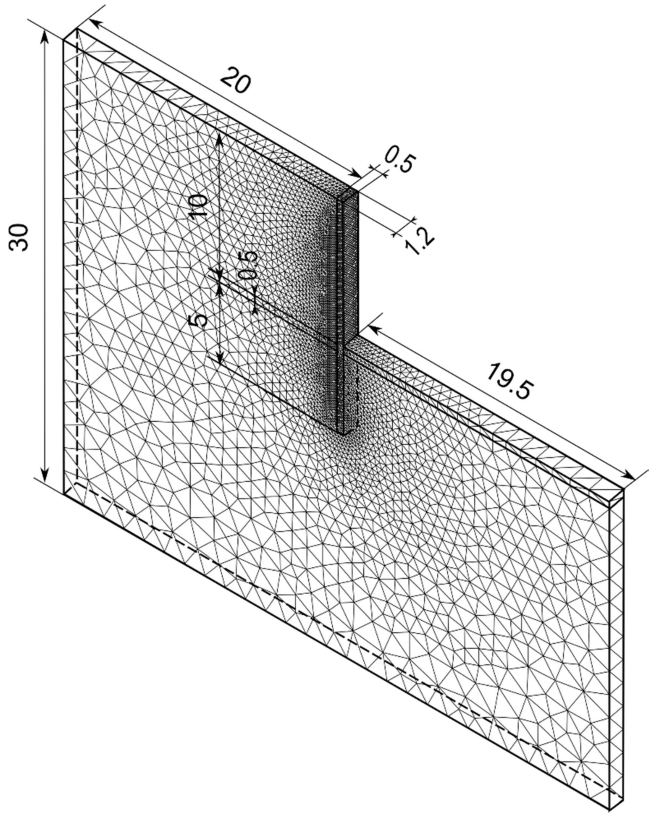

Figure 6. Geometry and sizes of the modelled domain with the finite element mesh (units m)

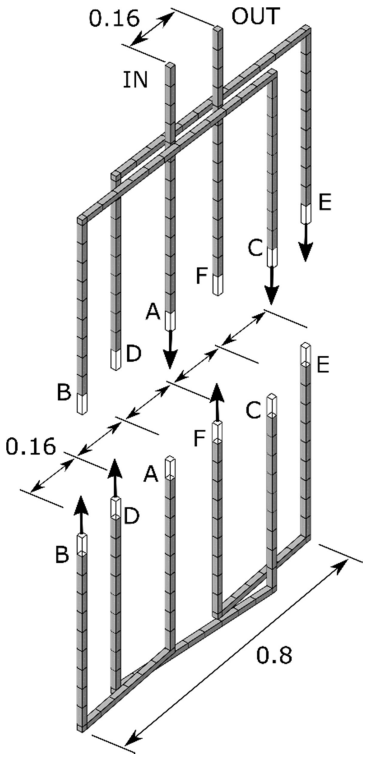

Figure 7. Details and finite element mesh for the left-side heat exchanger pipe in the base layout, located in the left pipe area shown in Figure 2 (units m)

In absence of both on-site and laboratory thermal characterization, the saturated soil properties are calculated as arithmetic means of the properties of solid and water components, weighed by the volume fractions [18,19]. An average porosity equal to 0.47 is assumed from surveying reports and the properties of the solid grains are based on literature data [e.g. 20-22]. For the reinforced concrete structures a similar approach is followed, considering the reinforcing steel fraction of 2.4%. Table 2 reports the thermo-physical properties of the various materials. Porosity and water content are assumed constant throughout the uncoupled thermal process, therefore the derived thermal properties remain constant. Table 2 reports also the properties of a sandy soil in dry conditions, taken from design standards [22], and of a reinforced concrete with a steel fraction equal to 1%, whose properties are calculated once again as the weighted average between the properties of steel and concrete. The latter values are adopted in the sensitivity analyses discussed in Section 5.2.

		Density ρ [kg/m^3]	Thermal cond. λ [W/(mK)]	Specific heat c [J/(kgK)]
Water/Heat carrier fluid		1000	0.57	4186
Solid grains		2750	3.6	820
Initial analysis	Saturated soil	1930	2.2	1642
	Reinforced concrete 2.4%	2500	2.6	880
Sensitivity analysis	Dry soil	1460	0.4	725
	Reinforced concrete 1%	2500	1.8	880

Table 2. Thermo-physical properties.

4.2 Thermal analysis

The thermal analysis is performed with the hypothesis of uncoupled hydro- and thermal processes. It is based on the energy balance condition and on the laws governing the heat transfer mechanisms, namely forced convection for the elements modelling the fluid in the exchanger pipe and conduction for those modelling the wall and the soil mass, where the hydrostatic regime allows to exclude heat convection. In fact in the saturated soil domain only heat transfer by conduction was assumed, as a first simplifying hypothesis supported by the evidence during the ground survey on site. This simplifying assumption can be considered acceptable given the good agreement between the monitoring data and the numerical results reported in section 5.

At the top boundary, the time-dependent conditions are assigned in the form of a given temperature, instead of given convective heat flux. Insights into the effects of applying the two different conditions can be found in [10]. The temperature conditions at the top boundary are derived from the ground surface temperatures monitored during 2015 by ARPA-Lombardia (Figure 8). The monthly temperature average is calculated for each month and the resulting temperature variation is applied at the ground surface boundary. A similar variation,

with same mean value (13.4°C) but amplitude damped by a coefficient of 0.66, is applied at the excavation boundaries. This assumption comes from the need to consider a unique representative thermal boundary condition for the entire set of wall panels, subjected to different conditions but generally all characterized by temperatures that are mitigated with respect to the atmospheric ones. The degree of mitigation is different for different panels, since some are exposed to the car ramp, open to a central aeration shaft, others are exposed to an empty gap designed for natural ventilation of the parking lot, others are not even connected with the outside. The latter is the condition of the base slab too, where the temperatures are even more mitigated with respect to the outside climate. The damping coefficient of 0.66 was obtained as optimal value to simulate the temperature variation monitored at the probes closest to the excavation surface (ES7 and ES9), during the first period of inactivity of the geothermal system, i.e. when the wall temperature is more representative of the undisturbed temperature of the basement.

The initial condition required by the numerical integration is set as the result of the simulation of a 5 year period of cyclic temperature variations at the ground surface and excavation boundaries. For this analysis, a representative yearly cyclic variation is assumed, computed as average over the period 2010-2015 from ARPA measurements. Preliminary analyses proved that a 5 years time span is sufficient, in this model, to reach the cyclic thermal equilibrium within the entire soil mass. This assumption entails that the construction time is long enough to let the temperature field reach the new equilibrium before activating the geothermal system.

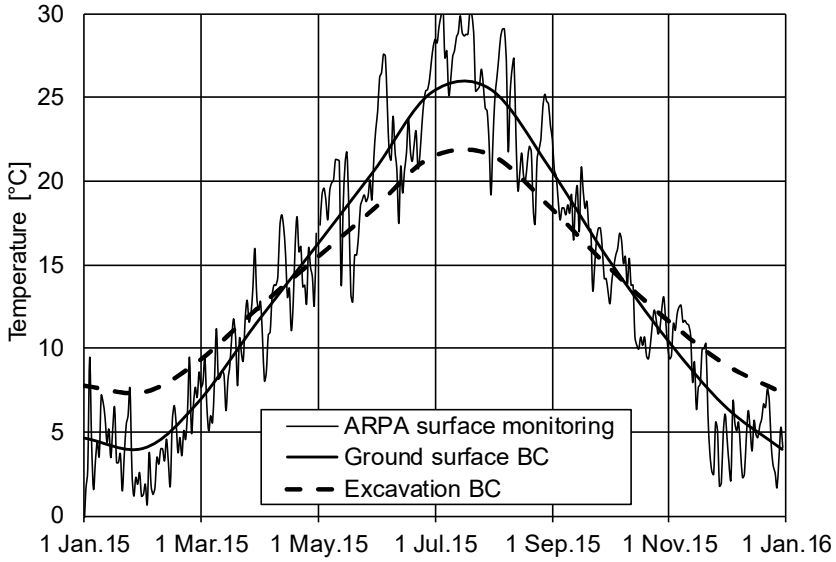

Figure 8. Monitored atmospheric temperatures (ARPA-Lombardia) and applied Boundary Conditions at the ground surface and at the excavation boundaries, with constant damping of 0.66.

The forced convection in the pipe is prescribed by assigning the mass flow rate, uniform along the pipe, and the fluid temperature at the pipe inlet (Figure 9). These input data are worked out from the monitored data, as average values over time intervals that depend on the operation mode of the geothermal system. Longer time intervals are admitted when the variables undergo minor variations, shorter intervals when they undergo rapid variations and when a refined simulation is needed. The latter is the case of December 2015, the period chosen for the calibration of the model for its continuous and stable heating operation mode. Figure 9, referring to the period from the beginning of the monitoring (2015 July 1st) to the end of the calibration month (2015 December 31st), shows that the input variables are worked out as averages on long periods, from July 2015 (starting date of the system) to November 2015, whereas they are more refined in December 2015.

The long idle period, from the last week of July to the end of August 2015, can be confirmed by the corresponding vanishing value of the mass flow rate, while high mass flow rates in December confirm the high heating demand of winter period.

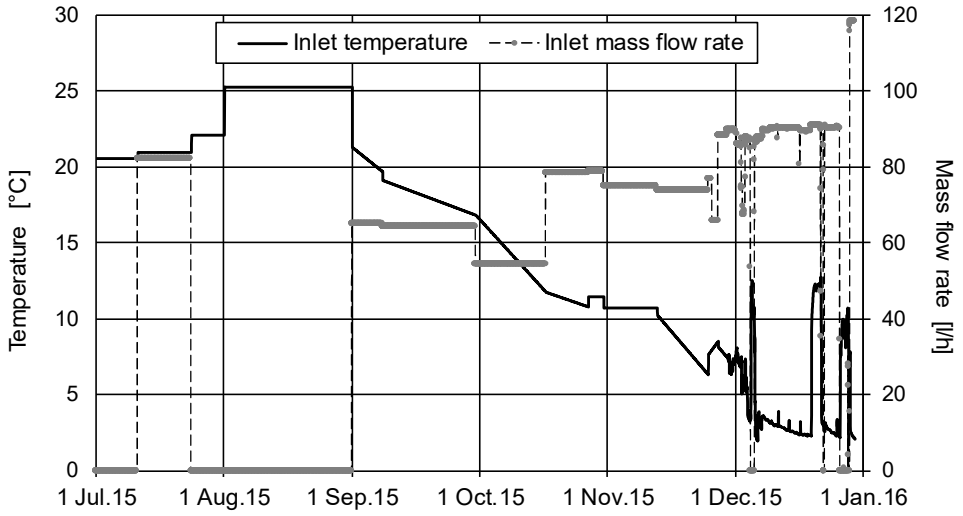

Figure 9. Fluid inlet temperature and mass flow rate as input data for the exchanger pipe.

5. Numerical results

5.1 Monitoring vs. numerical results

A comparison between monitoring and numerical results is here shown firstly with reference to the temperature variations, from July to December 2015, at representative positions within the soil mass and the wall: (i) along the anchor (probe AS2.5 in Figure 10), where the temperature is less influenced by the circulating fluid and the fluctuations are delayed and damped with respect to the thermal inputs on the wall, (ii) within the wall at the soil side (probe SS7 in Figure 11), where the influence is mostly due to the circulating fluid, and (iii) within the wall at the opposite side (probe ES7 in Figure 12), where conversely the influence is mostly due to the thermal condition at the excavation boundary.

The first comparison to be discussed is between the monitoring data (dots in Figures 10 to 12) and the numerical results as obtained from the model described in Section 4, referred to as Initial (solid black lines). The figures show a good agreement in the first months of operation,

but an overestimation of the temperatures by the numerical model starting with November, especially marked at position ES7, which is the closest to the excavation side (Figure 12). This result suggests investigating the influence of key parameters, such as the thermo-physical properties and the thermal boundary conditions, and possibly calibrating their values to obtain the best agreement with the monitoring data.

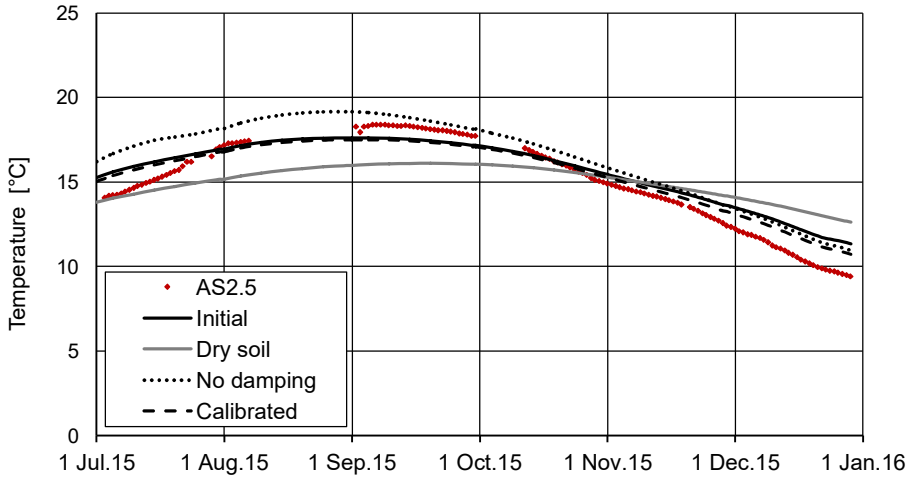

Figure 10. Temperature variation at probe AS2.5 from monitoring (dots) and numerical analyses (lines): Initial analysis, sensitivity analysis on soil properties (Dry soil), calibrated analyses on thermal boundary conditions (No damping and Calibrated damping)

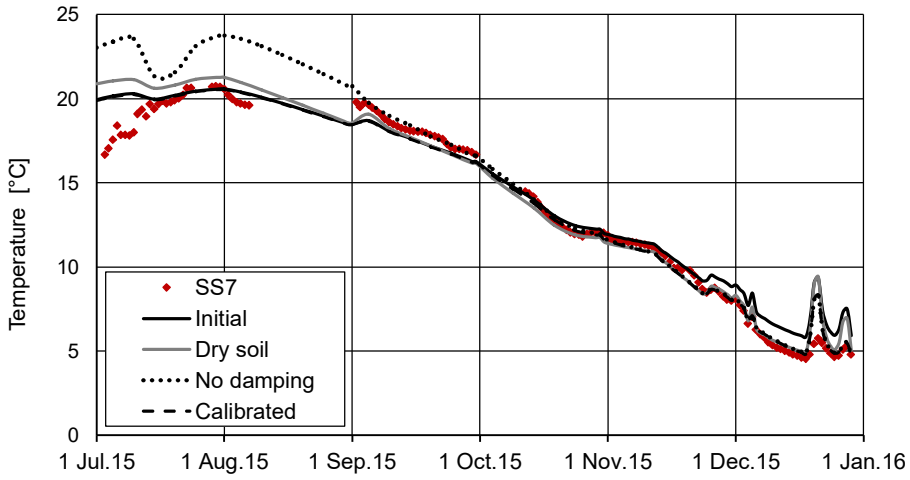

Figure 11. Temperature variation at probe SS7 from monitoring (dots) and numerical analyses (lines): Initial analysis, sensitivity analysis on soil properties (Dry soil), calibrated analyses on thermal boundary conditions (No damping and Calibrated damping)

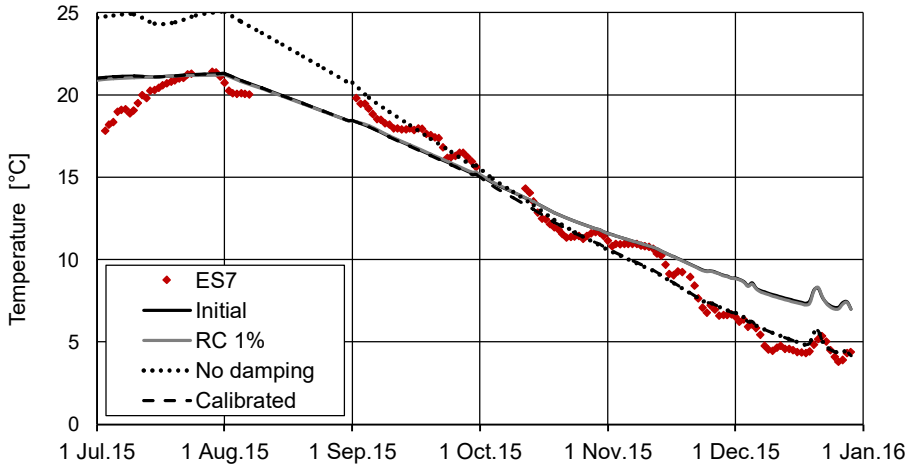

Figure 12. Temperature variation at probe ES7 from monitoring (dots) and numerical analyses (lines): Initial analysis, sensitivity analysis on Reinforced Concrete properties (RC with steel volume fraction of 1%), calibrated analyses on thermal boundary conditions (No damping and Calibrated damping)

5.2 Sensitivity analysis and calibration of the boundary conditions

In a first attempt to calibrate the model, the sensitivity to thermo-physical properties of the materials is investigated. From the one hand, the soil mass could be in a dry condition, from the other hand, the reinforced concrete wall could be designed with a lower fraction of reinforcing steel. Consequently, both materials could be characterized by lower values of thermal conductivity and/or specific heat. Table 2 reports the thermo-physical properties of a dry sandy soil [22] and of a reinforced concrete with 1% steel, used to perform additional numerical analyses.

The results show that the variation of the soil properties mainly leads to a worse agreement in the temperatures within the soil mass (grey line in Figure 10), while the temperatures of the wall remain rather unaffected, as expected, since they mainly depend on the temperature of the circulating fluid and of the excavation side (grey line in Figure 11). The assumption of a saturated condition, with thermo-physical properties based on site surveying and literature data, seems therefore acceptable for the simulation at hand. Conversely, the variation of the

reinforced concrete properties has no effect on the soil mass temperatures (data not shown) and in the wall temperatures (grey line in Figure 12).

As discussed in the Introduction, the thermal boundary condition applied at the excavation side is recognized as a major factor of influence in the numerical modelling [10,11,23,24]. The variability of this condition is used here to calibrate the numerical modelling, with the objective to reach a better agreement in the temperatures at positions close to the excavation side (ref. ES7 in Figure 12).

The damping coefficient of 0.66 used in the initial analyses allowed to simulate the temperature variations in the summer months (idle period for the geothermal system) with sufficient accuracy, as confirmed by the good agreement between monitored and calculated values. The assumption of a different damping coefficient could lead to a better or to a worse agreement in other periods of the year. As an example the extreme case of no damping (i.e. on the excavation boundaries the same temperature variations of the ground surface are applied, namely damping coefficient equal to 1), leads to a better agreement in winter time, but to a worse agreement in summer time, as shown by the dotted lines in Figures 10 to 12.

Removing the simplifying yet arbitrary hypothesis that the damping coefficient is constant over the year, a better agreement can be reached with all the monitoring data in the various periods. From the two previous analyses, with respectively constant 0.66 and constant unit coefficients, a combination of them is attempted, in which the damping effect of 0.66 is introduced for the summer period only (from May to September), while in the winter period the excavation temperatures are not damped with respect to the ground surface ones (from November to March). This assumption can be based on the consideration that the natural convection that takes place in the aeration space connected with the wall (the gap between the wall and the basement, or the ramp shaft) may help mitigating the elevated outdoor

temperatures in summer, but it has no effect in mitigating the low temperatures in winter. From this new calibrated analysis, the best agreement between monitoring data and numerical results is achieved, in both summer and winter time, as shown by the dashed lines in the same Figures 10 to 12.

Finally, a comparison in terms of fluid temperatures at the pipe outlet is also necessary, as a measure of the monitored vs. predicted heat rate and energy performance. Figure 13 reports this result focusing on December month. The initial model overestimates the temperatures at the outlet in all the days of operation of the system; whereas in the idle periods, when the inlet temperature naturally increases, the rise of temperature at the outlet is lower than the measured one. Integrating over the days of effective operation, in December the initial model predicts a heat exchange of the single pipe equal to 223 kWh, for about 600 h of operation, i.e. an average heat rate of 371 W and a specific heat rate over unit wall surface of 20.6 W/m^2 (ref. first row of Table 3). These values are a 38% overestimation of the measured performance, equal to 14.9 W/m^2 (Table 1). On the contrary the calibrated model, characterized by a lower boundary condition temperature at the excavation side, results in outlet temperatures that are lower and in good agreement with the measured values (Figure 13). The corresponding monthly heat exchange is 157 kWh, with average heat rate of 263 W and specific heat rate of 14.6 W/m^2, that slightly underestimates the measured value by 2%.

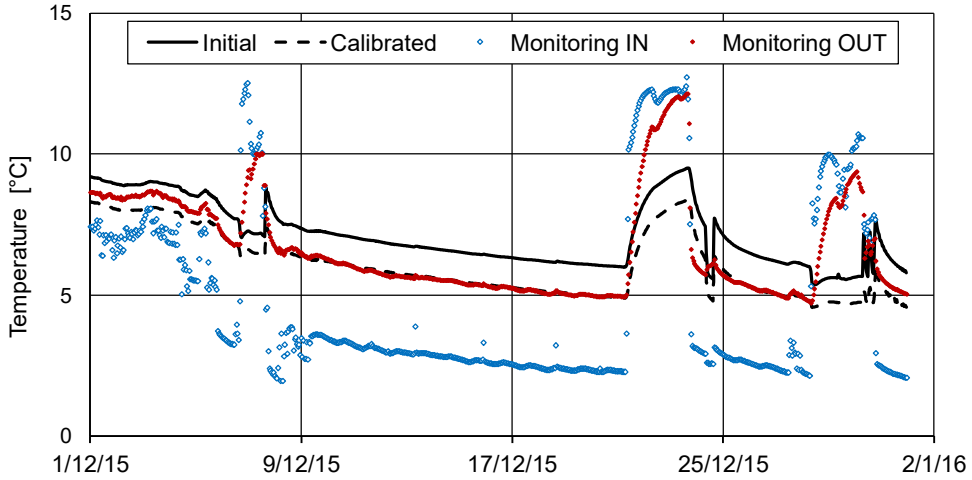

Figure 13. Fluid temperature variation at the pipe outlet in December 2015 from monitoring (dots) and numerical analyses (lines): Initial analysis and calibrated analysis on thermal boundary conditions

5.3 Optimization of the loop layout

In the numerical analysis, the explicit modelling of the fluid within the exchanger pipe and of the forced convection allows to analyze the detail of the heat transfer and temperature changes along the pipe length. Figure 14 shows the temperature change from the inlet (x=0) to the outlet (x=90 m) of the pipe, and the temperature gradient computed every 5 m of pipe length. Each 15 m of pipe length along the abscissa represent one of the six vertical branches forming the entire loop (labelled from A to F in Figure 7). The results refer to a representative day of December (10/12/2015) and are computed by means of the initial and of the calibrated models.

From the qualitative trend, similar for the two models, it can be observed that the thermal interferences between the vertical branches, 16 cm apart each other, govern the temperature changes. In fact, the greatest temperature increase occurs in the first three branches (A-B-C), because they all run close to branches where warmer fluid circulates: for instance, the first branch A (0-15 m) is confined between the fourth branch D and the last branch F, where the fluid is warmest. Conversely, branch D (45-60 m) turns out to be confined by two colder

branches (the first A and the second B) and, consequently, the thermal interference induces in it a decrease in temperature. The fifth branch E (60-75 m) takes advantage from being at the side of the loop, where it can harvest heat; whereas the last branch F (75-90 m) interacts with the colder first A and third C branches, and consequently it loses heat.

The difference between the results from the two models can be established on a quantitative base by the temperature gradients (dots in Figure 14). The markedly different values calculated in the first branches, up to about 40 m, highlight the influence of the imposed temperature at the excavation side, which is lower in the calibrated model (5.7°C) than in the initial one (8.5°C). Note that the difference is particularly evident in the portions 0-10 m, 20-40 m, and 60-70 m, where the pipe is not fully embedded but exposed to the excavation. Note also that, in the initial model, there is a uniform heat flux direction, from the excavation side to the fluid, because the wall surface temperature (8.5°C) is higher than the fluid temperature all over the exposed surface; whereas in the calibrated model the heat flux is not uniformly directed from the excavation side to the fluid, the wall surface temperature (5.7°C) being lower than the fluid temperature at some positions.

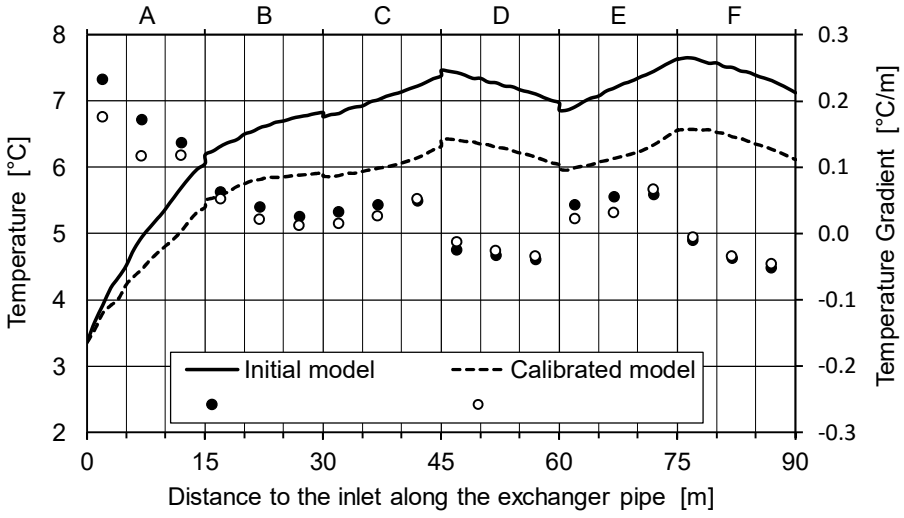

Figure 14. Temperature distribution (lines) and gradient (dots) along the exchanger pipe for the initial and the calibrated models, on 10/12/2015. Labels on the top indicate the 6 different branches of the pipe (see Figure 7).

As a result, it appears that two aspects are relevant for enhancing the heat exchange, namely increasing the distance between pipe branches circulating the fluid at different temperatures and minimizing the length of the path exposed to the excavation that, in some conditions, can negatively affect the heat exchange.

To improve the performance of the heat exchanger an attempt is made to redesign the pipe layout taking the above observations into account. Two enhanced layouts are proposed: the first features a single descending and a single ascending branch, kept at a distance from each other, and a W-shaped loop which remains in the fully embedded part of the wall (Figure 15). Note that, below excavation level, the full width of the half wall can be used for placing the loop, i.e. 1.2 m instead of 0.8 m, since there are no central perforations required for anchors installation (Figure 2). The distance between the vertical branches of the W-shaped loop is maintained to about 0.33 m to permit the safe bending of the pipe. This layout should limit the interference between coldest and warmest branches and the influence of the temperature of the excavation boundary. The total length of the Single-W layout is about 40 m, i.e. 45% of the length of the base layout.

The second enhanced layout has similar features with an additional W-shaped loop placed on the opposite side of the reinforcing cage, devised to benefit from the other face of the wall, which is in direct contact with the soil mass (Figure 16). As on the first face, also on the opposite one the distance between the loop and the soil is equal to the concrete cover (5-8 cm). The total length of the Double-W layout is about 60 m, i.e. 67% of the length of the base layout.

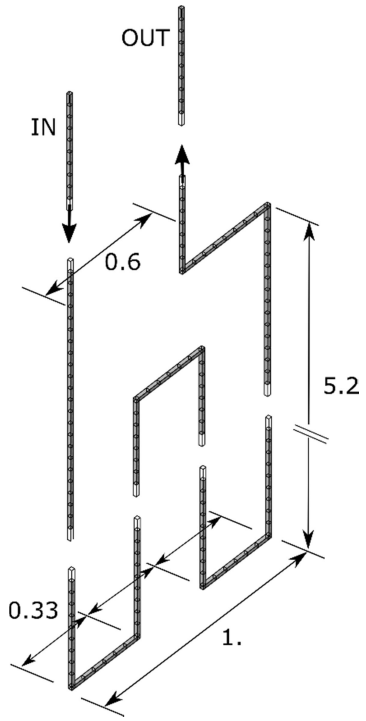

Figure 15. Layout of the enhanced Single-W heat exchanger pipe (units m)

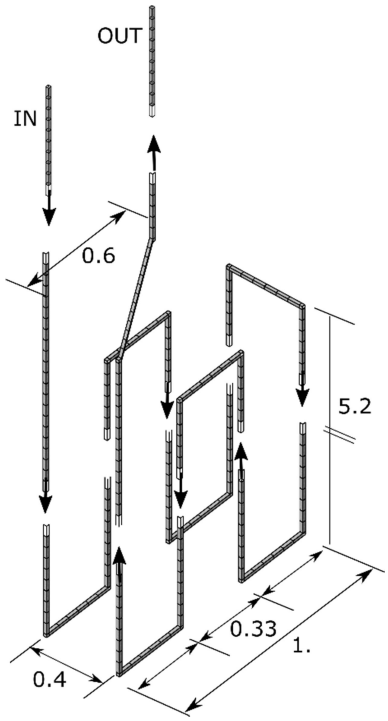

Figure 16. Layout of the enhanced Double-W heat exchanger pipe (units m)

The results of the numerical analyses are discussed in terms of fluid temperature change along the pipe length and compared with the case of the base layout, for the initial model and the calibrated one (Figures 17-18).

For both enhanced layouts, the fluid temperature undergoes a rather continuous increase as result of the negligible interference between branches at very different temperatures, especially the first and the last, now being 0.6 m apart from each other. The Single-W layout is limited by a rather short length (40 m) and, consequently, its outlet temperature remains lower than the one reached in the case of the longer Double-W layout (60 m). In both cases, the negative influence of a low thermal condition at the excavation side is confirmed by the lower temperature increase observed in the calibrated model with respect to the initial model, in the first (0-10 m) and last (30-40 m or 50-60 m) pipe segments exposed to the excavation.

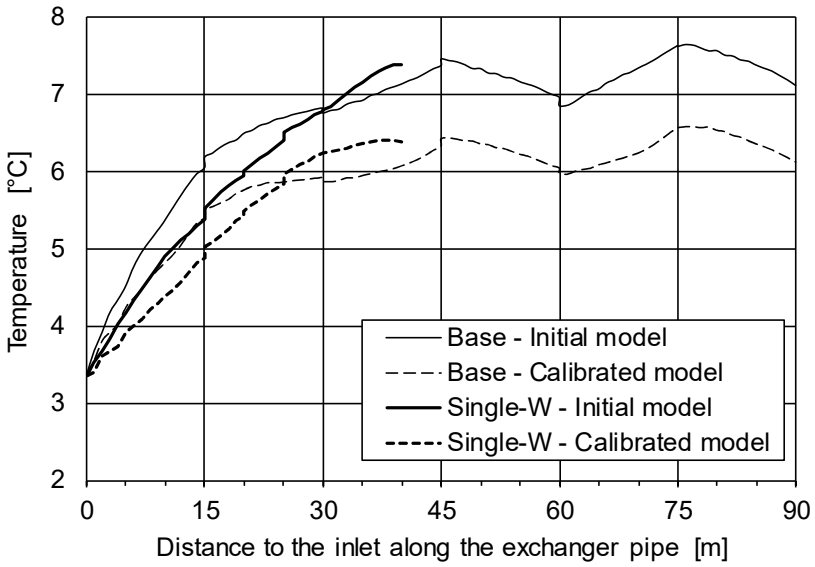

Figure 17. Temperature distribution along the enhanced Single-W exchanger pipe, compared with the base loop case, for the initial and the calibrated models, on 10/12/2015.

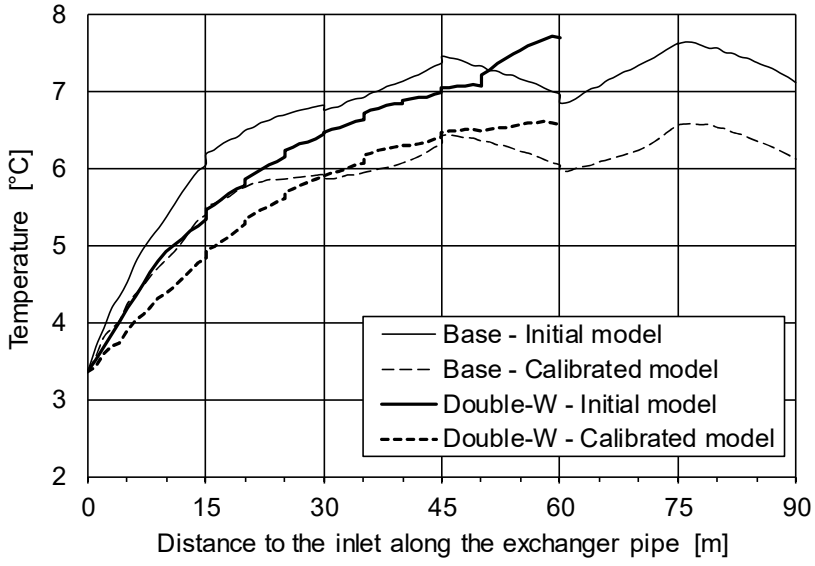

Figure 18. Temperature distribution along the enhanced Double-W exchanger pipe, compared with the base loop case, for the initial and the calibrated models, on 10/12/2015.

The energy performances of the three different layouts are compared in Table 3, in terms of total exchanged heat E, average heat rate q, and specific average heat rate q/S_{dw} per unit panel

wall surface (total area equal to 18 m^2), in December 2015. The slightly better performance of the Single-W layout compared to the base one (+6.6% in the initial model, +10% in the calibrated model, as average heat rate) demonstrates that a long piping is unnecessary if the thermal interference among branches is not minimized and the fluid circulates mostly above the excavation level. The markedly better performance of the Double-W layout (+14.5% in the initial model, +15.8% in the calibrated model) basically is the result of a longer pipe and of using both embedded faces of the wall.

Layout	Length [m]	E [kWh]		q [W]		q/S_{dw} [W/m^2]		Δq with respect to Base layout [%]	
		Initial	Calibrated	Initial	Calibrated	Initial	Calibrated	Initial	Calibrated
Base	90	223	157	371	263	20.6	14.6	-	-
Single-W	40	238	173	395	289	22	16.1	+6.6	+10.0
Double-W	60	255	182	425	304	23.6	16.9	+14.5	+15.8

Table 3: Energy performance of the three pipe layouts in December 2015, from the initial and the calibrated models

6. Conclusions

From the field monitoring of the Tradate building energy walls and slab, energy performance figures have been derived showing that the diaphragm walls exchange on average about 14 W/m^2, namely 2.7 times the base slab. The different heat transfer capacity of the two geostructures can be attributed to the boundary condition on the excavation side, impacting entirely on the slab area but only on 2/3 of the diaphragm walls area. Field observations actually suggest that the overall energy performance of the diaphragm walls results from the combination of the below excavation and the above excavation portion performance, the latter being influenced by a critical boundary condition, tentatively identified with the outdoor temperature profile damped by a proper factor.

The sensitivity analysis of the finite elements numerical model of the energy wall panel has shown that the reinforced concrete thermal-physical properties have marginal influence, while soil properties mainly affect the temperature variations into the soil. In turn the boundary condition on the excavation side has the major impact on the wall and heat transfer fluid temperatures. Following, the numerical model has been calibrated against measured data by adopting a boundary condition with a seasonally varying damping factor. The deviation between calibrated model predictions and measured data in terms of wall average heat rate is 2%, namely a very good agreement has been achieved.

By means of numerical modelling two alternative piping layouts have been investigated with the aim to maximize the energy performance of the energy wall. The innovative pipings are designed by minimizing thermal interference among the pipe branches with a significant temperature difference and by taking advantage of the fully embedded portion of the diaphragm wall. The simulation show that the Single-W layout and the Double-W layout can exchange 10.0 % and 15.8 % more heat than the base layout, with a pipe length equal to 45% and 67% of the base layout respectively.

7. Acknowledgements

The Authors gratefully acknowledge Giuseppe Bertani, F.lli Bertani srl and Lino Todeschini, Tecnoel srl for sharing the technical information and the monitored data of the Tradate building HVAC system.

References

[1] J.W. Lund, T.J. Boyd, Direct utilization of geothermal energy 2015 worldwide review, Geothermics 60 (2016) 66-93.

[2] EU Parliament, 2010/31/ED, Directive on Energy Performance of Buildings (EPBD), Bruxelles.

[3] P. Blum, G. Campillo, T. Kolbel, Thermo-economic and spatial analysis of vertical ground source heat pump systems in Germany, Energy 36 (2011) 3002-3011.

[4] H. Brandl, Energy foundations and other thermos-active ground structures, Geotechnique 56, vol. 2 (2006) 81-122.

[5] D. Adam, R. Markiewicz, Energy from earth-coupled structures, foundations, tunnels and sewers, Geotechnique 59, Vol. 3 (2009) 229-236.

[6] L. Laloui, A. Di Donna, Energy Geostructures: Innovation in Underground Engineering. ISTE Ltd, London, UK, 2013.

[7] P. Bourne-Webb, S. Burlon, S. Javed, S. Kurten, F. Loveridge, Analysis and design methods for energy geostructures, renewable and Sustainable Energy Reviews 65 (2016) 402-419.

[8] COST Action TU1405: European network for shallow geothermal energy applications in buildings and infrastructures (GABI), www.foundationgeotherm.org.

[9] M. Sun, C. Xia, G. Zhang, Heat transfer model and design method for geothermal heat exchanger tubes in diaphragm walls, Energy and Buildings 61 (2013) 250-259.

[10] P.J. Bourne-Webb, T.M. Bodas Freitas, R.A. da Costa Goncalves, Thermal and mechanical aspects of the response of embedded retaining walls used as shallow geothermal heat exchangers, Energy and Buildings 125 (2016) 130-141.

[11] A. Di Donna, F. Cecinato, F. Loveridge, M. Barla, Energy performance of diaphragm walls used as heat exchangers. Proceeding Institution Civil Engineers – Geotechnical Engineering, ICE Publishing, 170 (2017) 232-245.

[12] C. Xia, M. Sun, G. Zhang, S. Xiao, Y. Zou, Experimental study on geothermal heat exchangers buried in diaphragm walls, Energy and Buildings 52 (2012) 50-55.

[13] T. Amis, C.A.W. Robinson, S. Wong, Integrating Geothermal Loops Into The Diaphragm Walls Of The Bulgari Hotel Knightsbridge, Proceeding 11th DFI / EFFC Int. Conf. London, p. 10, 2010.

[14] D. Sterpi, A. Angelotti, D. Corti, M. Ramus, Numerical analysis of heat transfer in thermo-active diaphragm walls, Proc. 8th Eur. Conf. Numer. Methods Geotech. Eng. NUMGE 2014, 1043–1048, 2014.

[15] H. Brandl, Thermo-active Ground-Source Structures for Heating and Cooling, Procedia Engineering 57 (2013) 9-18.

[16] S. Kurten, D. Mottaghy, M. Ziegler, Design of plane energy geostructures based on laboratory tests and numerical modelling, Energy and Buildings 107 (2015) 434-444.

[17] Dassault Systèmes. Abaqus 6.14 Software Documentation. Dassault Systèmes Simulia Corp., Providence, RI, USA, 2014.

[18] S.W. Rees, M.H. Adjali, Z. Zhou, M. Davies, H.R. Thomas, Ground heat transfer effects on the thermal performance of earth-contact structures. Renew. Sust. Energ. Rev. 4 (2000) 213-265.

[19] A. Vieira et al., Characterisation of ground thermal and thermo-mechanical behaviour for shallow geothermal energy applications. Energies 10 (2017) 2044.

[20] D. Hillel, Introduction to environmental soil physics. Elsevier, 2003.

[21] H.R. Thomas, S.W. Rees, Measured and simulated heat transfer to foundation soils. Géotechnique 59 (2009) 365-375.

[22] UNI 11466:2012. Sistemi geotermici a pompa di calore – Requisiti per il dimensionamento e la progettazione (Heat pump geothermal systems - Design and sizing requirements), 2012.

[23] K. Soga, Y. Rui, D. Nicholson, Behaviour of a thermal wall installed in the Tottenham Court Road station box. Proc. Crossrail Conference, Crossrail Ltd and Federation of Piling Specialists, London (2015) 112-119.

[24] Y. Rui, M. Yin, Thermo-hydro-mechanical coupling analysis of a thermo-active diaphragm wall. Can. Geotech. J. 55 (2018) 720-735.